



Influence of quenching conditions on texture and mechanical properties of ultra-high-strength steels

Raphael Esterl^{1,*} , Markus Sonnleitner² , Irmgard Weißensteiner³ , Karin Hartl¹ , and Ronald Schnitzer¹ 

¹Department of Materials Science, Montanuniversität Leoben, Franz Josef-Str. 18, 8700 Leoben, Austria

²voestalpine Stahl GmbH, voestalpine-Straße 1, 4020 Linz, Austria

³Christian Doppler Laboratory for Advanced Aluminum Alloys, Chair of Nonferrous Metallurgy, Montanuniversität Leoben, Franz Josef-Str. 18, 8700 Leoben, Austria

Received: 7 March 2019

Accepted: 23 June 2019

Published online:

5 July 2019

© The Author(s) 2019

ABSTRACT

Direct quenching of thermomechanically processed low-carbon steels is a preferred production route to increase strength and toughness of ultra-high-strength steels and thus enhance the payload-to-weight ratio, e.g., of mobile cranes. However, during hot rolling, certain crystallographic textures emerge, which can generate unfavorable mechanical properties or mechanical anisotropy. In order to investigate the role of the processing route and the effect of micro-alloying elements on the texture formation and its relationship to differences between different testing directions, four different ultra-high-strength steels were subjected to various quenching procedures. It was found that despite equiaxed prior austenite grains after re-austenitization, differences in the longitudinal and transverse directions remain. The extinction of a rolling texture after re-austenitization is dependent on the austenitization condition and the addition of micro-alloying elements. In particular, Nb promotes the formation of rolling texture components and prevents the extinction thereof even through intense austenitization treatments. However, remaining preferred orientations exhibit only little influence on the anisotropy of the mechanical properties.

Introduction

For the production of mobile crane booms, ultra-high-strength steels (UHSS) are in application to provide an optimized payload-to-weight ratio [1–3]. The strength is accomplished by a grain refinement by means of a systematic combination of micro-alloying elements (MAE) and process parameters. This

includes as well a targeted temperature control during hot rolling [4–6]. A martensitic microstructure achieved through a subsequent quenching delivers a yield strength (YS) up to 1500 MPa [1, 3, 7–9]. The fine-grained microstructure not only meets highest strength requirements but also guarantees proficient toughness [3, 10]. UHSS produced via thermomechanical processing (TMP) have widely substituted

Address correspondence to E-mail: raphael.esterl@unileoben.ac.at

steels, which are fabricated through the conventional re-austenitization and quenching (RQ) route. High deformation rates in the non-recrystallizing austenite (γ) region provide enhanced refinement during the following transformation to martensite (α' = distorted α), thus offering further benefits in strength and toughness [1, 4, 6, 11].

The influence of the processing route on the mechanical properties has been broadly investigated [1, 5, 9, 10, 12–16]. A proportional correlation exists between the dimension of the austenite grain prior to the martensitic transformation and the emerging substructure such as blocks and packets [17–19]. Furthermore, increased reduction in the non-recrystallization region promotes the austenite pancaking and thus a finer microstructure during γ to α' transformation [1, 20–22]. These effects are exploited in steel production to optimize the mechanical properties. Nevertheless, it is also known that after hot rolling certain features remain in the microstructure, which results in an anisotropy of the mechanical properties [23]. On the one hand, nonmetallic inclusions lead to insoluble inclusion ligaments during rolling and thus affect differences in the longitudinal (L) and transverse (T) directions [23, 24]. However, process optimizations in the secondary metallurgy are nowadays capable of limiting these disadvantages through an adjustment of the inclusion structure [23–26]. Notwithstanding the mentioned positive effects on the mechanical properties, on the other hand, an increased reduction below the non-recrystallization temperature (T_{NR}) is also known to provoke the L – T anisotropy [20]. In a previous work, we showed that RQ does not eliminate the L – T anisotropy despite a equiaxed PAG [10]. From these observations it can be concluded that in fact the reduction in the non-recrystallization region, but not the shape of the PAG, influences the mechanical anisotropy. It has been observed that process parameters and MAE influence the inheritance of several characteristics, so that the newly recrystallized austenite grain has the grain size, shape and orientation of the previous microstructure [27, 28]. Several researchers have found that typical texture components of a α -fiber ($\langle 110 \rangle \parallel RD$) such as $\{001\} \langle 110 \rangle$, $\{112\} \langle 110 \rangle$ and $\{111\} \langle 110 \rangle$ can lead to unfavorable properties [20, 29–33]. These rolling texture components have detrimental effects on the bending properties including deviations of L and

T . In this case, the finish rolling temperature (FRT) possesses a major influence.

In order to gain a deeper insight into the L – T anisotropy, the present work establishes possible correlations between the differences in the mechanical properties and a preferred texture arising during rolling. For this matter, four direct-quenched UHS steels with different contents of MAE were investigated. Their mechanical properties in L and T were characterized and compared to the corresponding properties after RQ. In order to answer the question, if the re-austenitization conditions have an influence on these properties, three different heat treatments with varying austenitization temperatures and cooling times were performed before quenching. X-ray diffraction (XRD) measurements were taken to study the texture developments as a result of the performed heat treatments. The present work should shed light on the anisotropy of hot-rolled steels and help to understand the role of MAE and processing route on the formation of an unfavorable texture resulting in differences of the mechanical properties between L and T .

Materials investigated and experimental procedure

Materials, heat treatment and mechanical testing

The investigations on the influence of the processing route were performed on four different steels. These steels display industrial available UHS steel grades, which were provided from the coil as 6-mm-thick sheets. Their chemical composition is listed in Table 1. All steels experienced the same rolling conditions, and the FRT amounted 850 °C. The steels were labeled according to their strength classes and are numbered from 1 to 4. Steels 1 and 2 represent temper-resistant UHS steels and possess a carbon content of 0.09%. Additions of Mn, Si and B retard the γ to α transformation to ensure a martensitic microstructure [34–38]. Mo and V facilitate a TM process route through an elevation of T_{NR} [22, 34, 39, 40]. Moreover, they compensate for the softening during tempering and enhance weldability [41]. Compared to the base alloy 1, steel 2 has higher additions of Cr, and additionally, Ni is added for further temper resistance [37, 42]. Alloy 3 represents

Table 1 Chemical composition of the steels investigated (m%)

Steel	Description	C	Si	Mn	Cr	Ni	Mo	Cu	V	Ti	Nb	B
1	0.09 C, base alloy	0.09	0.1	1.6	0.70	0.01	0.20	0.03	0.10	0.02	< 0.01	0.002
2	0.09 C, increased alloy content	0.09	0.1	1.6	0.90	0.50	0.20	0.03	0.10	0.02	< 0.01	0.002
3	0.17 C, lean alloy	0.17	0.2	2.3	0.30	0.01	0.02	0.03	0.001	0.02	< 0.01	0.002
4	0.17 C, increased alloy content	0.17	0.3	1.4	0.70	1.0	0.40	0.50	0.05	0.02	0.04	< 0.001

a wear-resistant steel with a carbon content of 0.17%. Elevated additions of Si and Mn enable a through hardening [35]. Compared to steel 3, temper resistance is given in steel 4 with elevated amounts of Cr, Ni, Mo and Cu. Further, steel 4 is alloyed with Nb, which serves as strongest MAE in retarding recrystallization and providing additional strength after tempering [10, 43].

The steels were investigated in the as-rolled condition and compared to re-austenitization and quenching, for which three different austenitization procedures were performed. The different heat treatments are listed in Table 2. The conventional re-austenitization and quenching (RQ) consists of an austenitization at a temperature of 930 °C for 5 min followed by water quenching. In the second route, quenching is performed after normalization treatment and an extended austenitization time of 30 min (NRQ). In the third route, quenching was executed after a higher austenitization temperature of 1050 °C (HRQ).

Tensile tests were performed according to DIN EN ISO 6892-1 on flat tensile specimens in longitudinal and transverse directions of the 6-mm-thick sheet of each condition. The notch impact tests at 0°, – 20 °C and – 40 °C were performed according to DIN EN ISO 148-1 on 6-mm-thick specimens, and the obtained notch impact work was standardly converted to 10 × 10 mm full-sized samples by linear upscaling. Tensile tests were applied twice in each direction,

and for impact tests, three samples of each condition were tested.

Sample preparation and parameters for XRD and EBSD analysis

For the microstructural analysis, three different conditions (DQ, RQ and NRQ) of the four steels were investigated. Since the measuring principles of XRD and EBSD differ, the perspective on the sheet is also different. The relevant position to detect rolling textures was set to one-fourth of the sheet thickness [44]. For EBSD measurements, the transverse direction (TD) of the sheet is observed, as the electron beam can be focused to the significant position on the sheet.

The samples were hot embedded and then ground from 320 grit to 4.000 grit SiC paper for at least 30 s. Subsequently, the samples were polished with 3 μm diamond paste for at least 3 min and with 1 μm for 30 s. A silicate polishing was used (*Struers OPS*) for 10 min prior to a finishing electrolytic ablation of 5 s with 35 V. The samples were dipped in a diluted Nital etchant and plasma cleaned for 9 h before performing EBSD measurements. The measurements were taken using a EDAX Hikari XP EBSD system, installed in a *FIB Versa FEI 3D DualBeam*. An acceleration voltage of 30 kV was applied, and a step size of 100 nm was chosen. The data acquisition was performed with *EDAX Team 32*. The data were evaluated with *EDAX OIM Analysis 7.3*, in which a

Table 2 Heat treatment and quenching procedures; T_Q displays the quenching time and t_Q the austenitization time

Description	1. Heat treatment			2. Heat treatment		
	T_Q (°C)	t_Q (min)	Cooling medium	T_Q (°C)	t_Q (min)	Cooling medium
DQ Direct-quenched			Water			
RQ Re-austenitized and quenched	930	5	Water			
NRQ Normalized, re-austenitized and quenched	930	30	Air	930	30	Water
HRQ High-temperature re-austenitized and quenched	1050	5	Water			

neighbor orientation correlation cleanup and grain dilatation cleanup with one single iteration were executed. High-angle grain boundaries with an angle of $> 10^\circ$ were highlighted. The misorientation distribution was analyzed in steps of 2° .

In contrast to the electron beam, the X-ray beam cannot be focused. Therefore, the surface of the sheet was milled down to one-fourth of the thickness prior to grinding and polishing in order to place the beam on the relevant position of the sheet. In the following, electrolytic polishing was performed for 1 min with 35 V. The utilized XRD, *Bruker D8 advance*, was operated with a voltage of 40 kV at 40 mA and a K_α Cu X-ray tube. In steps of 5° , {110}, {200} and {211} pole figures were measured by means of a *LYNXEYE XE* detector and evaluated with the program *DiFFRAC.SUITE.measurementTM*. The orientation distribution functions (ODF) of the individual sample conditions were calculated from the obtained pole figures in the software package *MTEX* at an applied half width of 5° [45]. Volume portions are then calculated to describe the relative volume of the relevant crystals, which obtain a certain orientation.

Results

Mechanical properties

The yield strength of the 4 steels investigated is provided in Fig. 1. Steels 3 and 4 possess significantly higher YS compared to steels 1 and 2. The strength of the DQ condition is considerably above those after re-austenitization (RQ) for each of the steels investigated. The additional normalization (NRQ) and the higher austenitization temperature (HRQ) result in a minor decrease in strength for steels 1 and 4. Yet, this phenomenon is less pronounced as compared to DQ. Steels 1 and 2 show higher YS in *T* than *L*, whereby these differences are decreasing after re-austenitization, NRQ and HRQ. The *L–T* differences between steel 3 and steel 4 show opposite tendencies, and the YS in *L* is little higher compared to *T*. The heat treatments, however, do not reveal a clear trend concerning the *L–T* anisotropy of the YS. Clearer differences in the *L–T* anisotropy are evident in the Charpy impact toughness, which are displayed in Fig. 2 for the investigated steels at a testing temperature of 0°C . The toughness behaves diametrical to

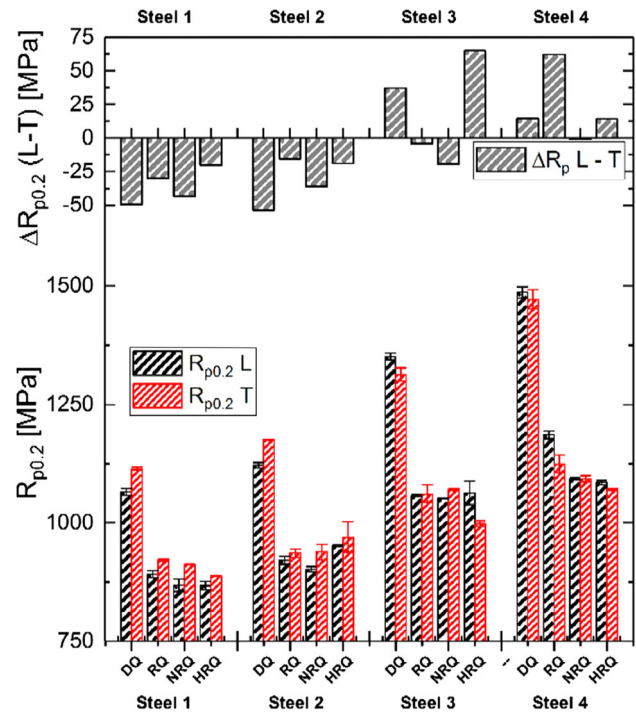


Figure 1 YS and *L–T* difference values dependent on the heat treatment of the four steels investigated. The strength decreases significantly through re-austenitization and quenching. Steels 1 and 2 improve regarding their *L–T* anisotropy; however, the differences are very little regarding the absolute UTS values of > 900 MPa. Steels 3 and 4 exhibit no clear trend.

the strength, and steels 1 and 2 have the highest Charpy impact toughness values, followed by steels 4 and 3. Steels 1–2 experience a deterioration of the impact toughness values through re-austenitization and quenching, steel 3 first after normalization. The toughness of steel 4, however, increases through re-austenitization. The *L–T* anisotropy of steels 1 and 2 benefits from the re-austenitization. The more intense the annealing in the γ region is (e.g., NRQ and HRQ), the smaller the *L–T* difference becomes. For steels 2, it disappears completely. The anisotropy for steels 3 and 4 is neither deteriorated nor improved through different treatments in the γ region. The temperature dependence of the Charpy impact toughness is displayed in Fig. 3 for temperatures between -40 and 0°C for steels 2–4. The decrease in the impact toughness of steel 2 is less pronounced at 0°C ; however, at -20°C , it deteriorates to values below 50 J. The impact toughness of steel 4 is clearly improved through re-austenitization and amounts even at -40°C almost 100 J for the normalized and quenched variant NRQ.

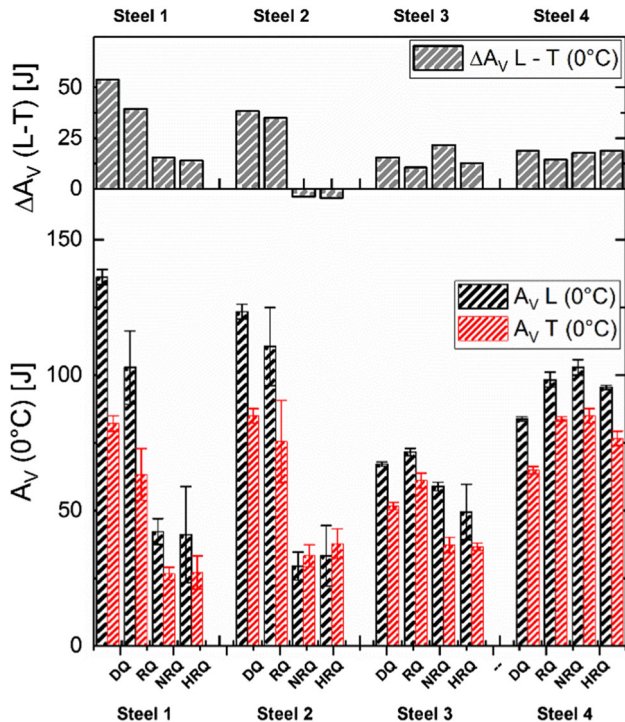


Figure 2 Charpy impact toughness values and $L-T$ difference values at 0 °C dependent on the heat treatment of the four steels investigated. Steels 1–3 experience a deterioration of the impact toughness through re-austenitization and quenching, whereas steel 4 delivers an improvement in toughness. The $L-T$ anisotropy of steels 1 and 2 seems to benefit from re-austenitization, whereas steel 4 does not show any reaction not even through high quenching temperatures.

EBSD analysis and boundary misorientation distribution

The inverse pole figure maps for steels 2–4 in the TD are given in Fig. 4. In the DQ condition, steels 2 (a) and 4 (c) show a strong deformation of the former γ -grains toward the rolling direction. Steel 4 exhibits a very fine martensitic microstructure, which is divided in blocks and laths, originates from the also very fine prior austenite grains. The martensitic microstructure of steel 3 originates from equiaxed PAGs, which are obviously larger than in steel 4. During re-austenitization, the PAGs form to a equiaxed shape, which is shown in Fig. 4d–f. Whereas steels 2 (d) and 3 (e) coarsen significantly through reheating in the γ -region, the grain growth of steel 4 is limited. Both the PAGs and the martensitic components are still extremely fine after re-austenitization.

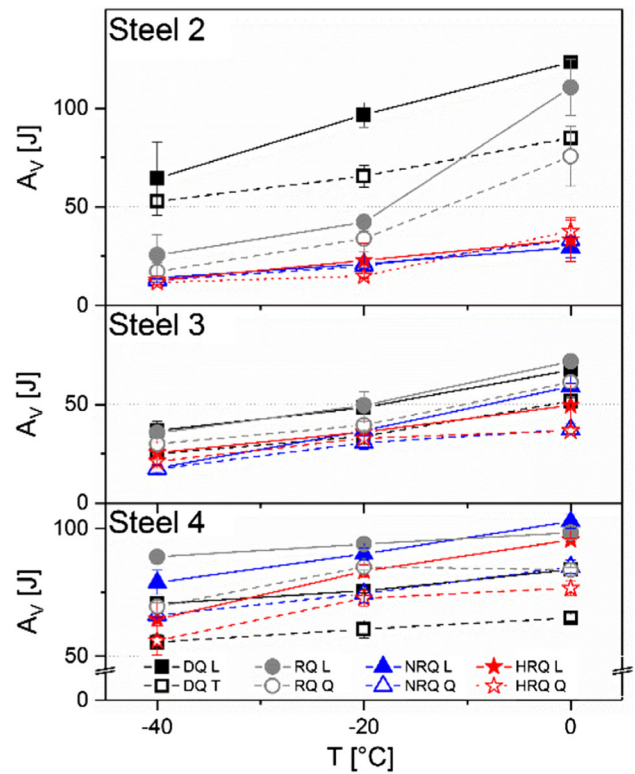


Figure 3 Charpy impact toughness between -40 and 0 °C for steels 2–4. Steel 2 deteriorates significantly through re-austenitization, whereas steel 3 does not show pronounced influence of the hardening treatment due to generally lower impact strength values. The impact toughness values of steel 4, which are already very high are little improved through both RQ and NRQ.

Figure 5 shows the distribution of misorientation angles of steels 2–4. Four peaks are visible in the distribution of all investigated specimen. Augmented peaks are found at 6.5° and 59.5° and peaks with weaker appearance at 17° and 53° . The magnification of the relevant positions of the diagram in Fig. 5 delivers an influence of the heat treatment on the frequency of these angles. Steels 2 and 4 show an increase in the intensity of the 6.5° —angles after RQ, compared to DQ. Steel 3 does not exhibit a change of this fraction after re-austenitization. At the misorientation at 59.5° , in particular steels 3 and 4 show higher fractions after RQ, and steel 2 only possesses a weak intensification.

XRD measurements: ODF maps and quantitative texture analysis

Figure 6 illustrates the ODF at a constant angle $\phi_2 = 45^\circ$ of steels 1–4 dependent on the processing

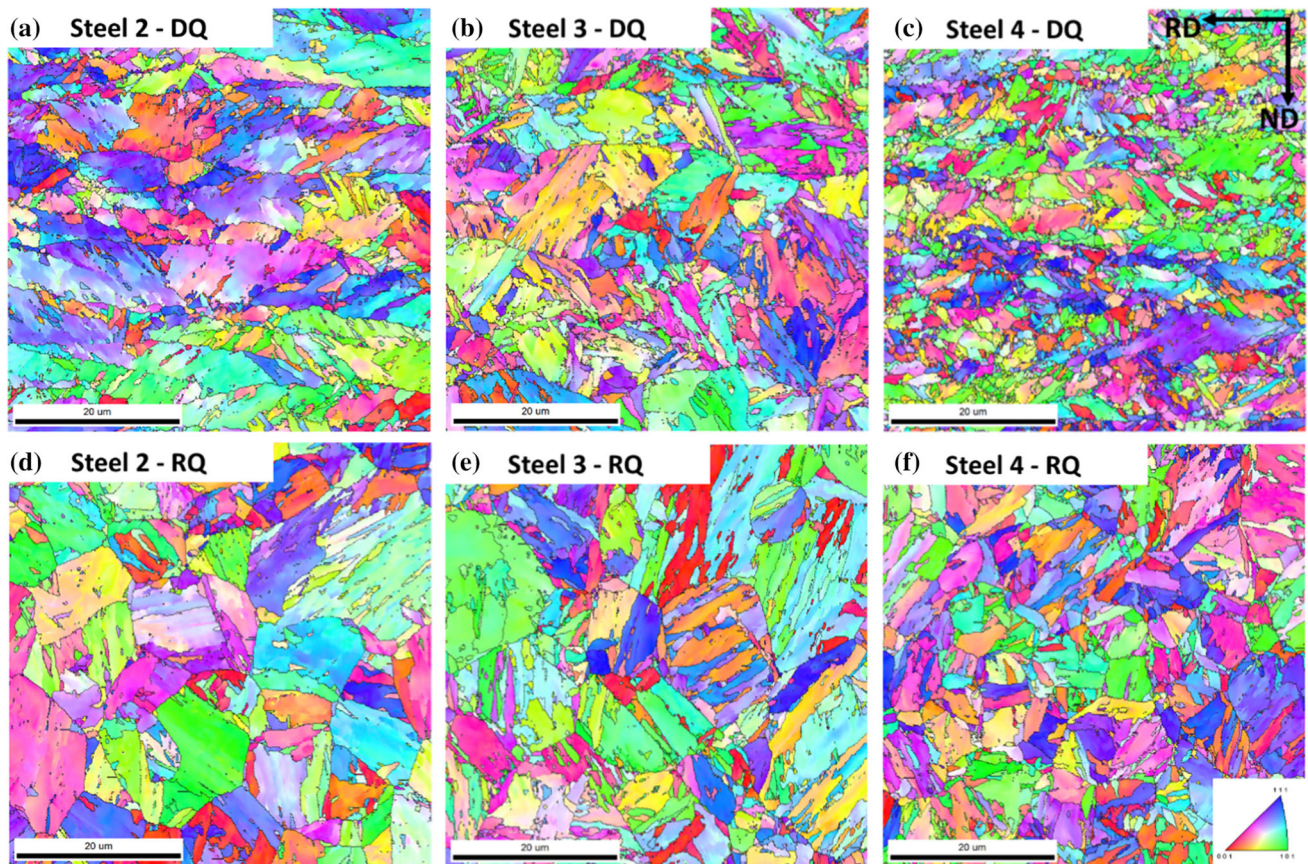


Figure 4 EBSD inverse pole figures with high-angle grain boundaries ($> 10^\circ$) for the TD in the as-rolled condition for **a** steel 2, **b** steel 3 and **c** steel 4. The MAE in steel 2 (**a**) and 4 (**c**) promote a pancaking toward the RD, and the PAGs are clearly visible as elongated grains. Steel 4 (**c**) exhibits the finest

microstructure (martensitic block and laths). Steel 2 (**b**) possesses equiaxed PAGs. **d–f** Although after re-austenitization and quenching (RQ) the PAGs increase and become equiaxed for **d** steel 2 and **e** steel 3, steel 4 (**f**) still maintains the finest microstructure.

condition. A significant increase in the rotated cube component $\{001\} \langle 110 \rangle$, evaluated from the ODF with an angular tolerance of 10° was observed for steels 1–3, especially in the DQ condition. The volume portions (Fig. 7) amount 10% for steels 1 and 2 and 11% for steels 3 and 4. During re-austenitization and quenching, all texture components decrease in favor of a slight increase in $\{112\} \langle 110 \rangle$. All texture components of steel 3 fall below 5% even after a single re-austenitization, concluding that only little fragments from the rolling history remain. In contrast to the aforementioned, steel 4 exhibits increased intensities in $\{111\} \langle 112 \rangle$, $\{112\} \langle 131 \rangle$ and $\{554\} \langle 225 \rangle$ after DQ. These components are marginally reduced on behalf of a growth of the $\{001\} \langle 110 \rangle$ constituent during RQ and NRQ. However, all texture components of steel 4 are still present to an increased extent.

Discussion

In order to investigate the influence of hardening and varying austenitization conditions on the mechanical properties, four low-C UHS steels were examined regarding their mechanical anisotropy and microstructure. These findings and their relevance are discussed in detail below.

Mechanical properties

The development of the YS revealed at first sight that an intense austenitization with a prior normalization can have a positive effect on the L – T anisotropy. Regarding the 0.09% C steels 1 and 2, the YS anisotropy behaves differently compared to steels 3 and 4. Steels 1 and 2 show higher YS in T than in L , whereas steels 3 and 4 show little higher YS in L . Due to the fact that the DQ strip is coiled after cooling and

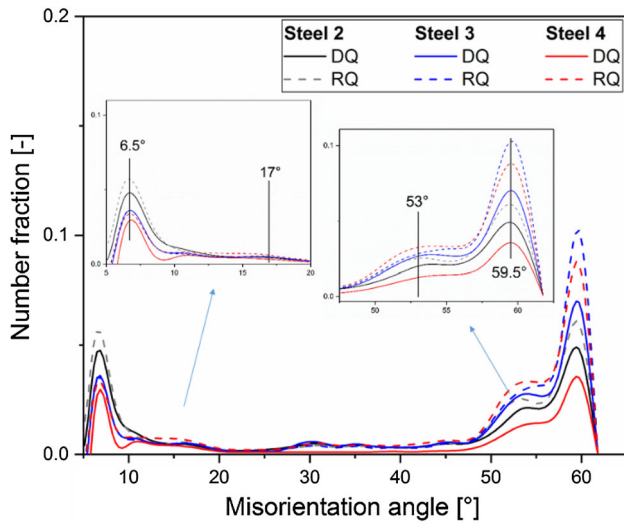


Figure 5 Grain boundary misorientation distribution of steels 2–4. Augmented peaks are identified at 6.5° and 59.5° , weaker peaks at 17° and 53° , respectively, for all specimens. The fraction of boundaries at 6.5° increases for steels 2 and 4 after re-austenitization. For steel 3, the fraction of DQ compared to RQ remains unaffected. All investigated specimens show an increased fraction of boundaries with 53° and 59.5° after re-austenitization, especially steels 3 and 4.

straightened prior to further processing, residual stress is induced. It is experienced that the more intense this straightening is, the lower the longitudinal YS becomes by the induced residual stresses. The transverse YS is not affected, as the strains are only applied along the rolling direction. The L – T anisotropy of the YS of steels 1 and 2 thus are disguised by these strains. The apparent decrease in the YS anisotropy after re-austenitization consequently can be associated with recovery. If steels 3 and 4 now are withdrawn from a rather outer part of the coil, the straightening is reduced due to the bigger coil radius, which subsequently leads to smaller residual stresses. This could explain the different behavior of steels 1 and 2 compared to steels 3 and 4. Nevertheless, the tensile tests have been performed on a *class 1 tensile testing machine*, which possesses an accuracy of 1%. Consequently, these deviations of the YS of steels 3 and 4 fall below the measuring tolerance so that this delivers no sufficient basis for interpretations of the L – T anisotropy. By re-austenitization, however, the absolute YS is significantly decreased. Regarding steel 1, the YS decreases by $\sim 17\%$, steels 2 and 3 by 20% and steel 4 even by 24% after a single re-austenitization in the T direction. These observations can be attributed to the grain

growth during re-austenitization, as depicted by the IPF map in Fig. 4, but cannot alone be the reason for this significant decrease. Although for all steels the YS is deteriorated in the same amount, the microstructure of steel 4 still maintains very fine after re-austenitization, whereas the grain size of steels 1–3 increase unambiguously. A detailed explanation can be given with a view to the different alloying concepts. All investigated steels were rolled with an FRT of 850°C . The rolling below T_{NR} leads to a high deformed γ grain (pancaking), which results in a very fine transformed microstructure. Nb (in steel 4) has a by far stronger effect than V (steels 1 and 2) to retard recrystallization [10, 21, 22, 34, 43, 46]. The consequence is that the strength contribution through TMP for steel 4 is much more augmented than compared to steels 1 and 2. Although the grain coarsening of steel 4 through RQ is less pronounced, the lack of a high deformed γ grain accompanied by the recrystallized austenite contributes to the 24% decrease in YS. These effects as well are observed in the temperature dependence of the Charpy impact toughness, which is displayed in Fig. 3. The detected grain coarsening of steel 2 not only reduces the impact toughness, but shifts the transition temperature to higher values. Although steel 3 is dispensed with alloying elements which are known to optimize the impact toughness (Mo, V, Ni) [41, 47], the toughness still is above 50 J at 0°C and does not deteriorate noticeably through re-austenitization. Steel 4 profits from the fine grain, which is still maintained after re-austenitization and results in higher impact toughness, which is even improved through RQ in elevating the entire level of the DBTT to higher toughness.

Microstructure and texture

The investigations on the microstructure delivered details on the different behavior of the four investigated low-C steels regarding their microstructure–property relationship. Several peculiarities of the mechanical properties have been explained through the grain size and structure by means of EBSD measurements. A view on the distribution of the misorientation angles (Fig. 5) gave further insight into the microstructure. Augmented peaks were observed at angles of 6.5° and 59.5° and peaks with weaker appearance at 17° and 53° for all investigated specimens. These peaks correspond to variants of the Kurdjumov–Sachs orientation relationship of packet,

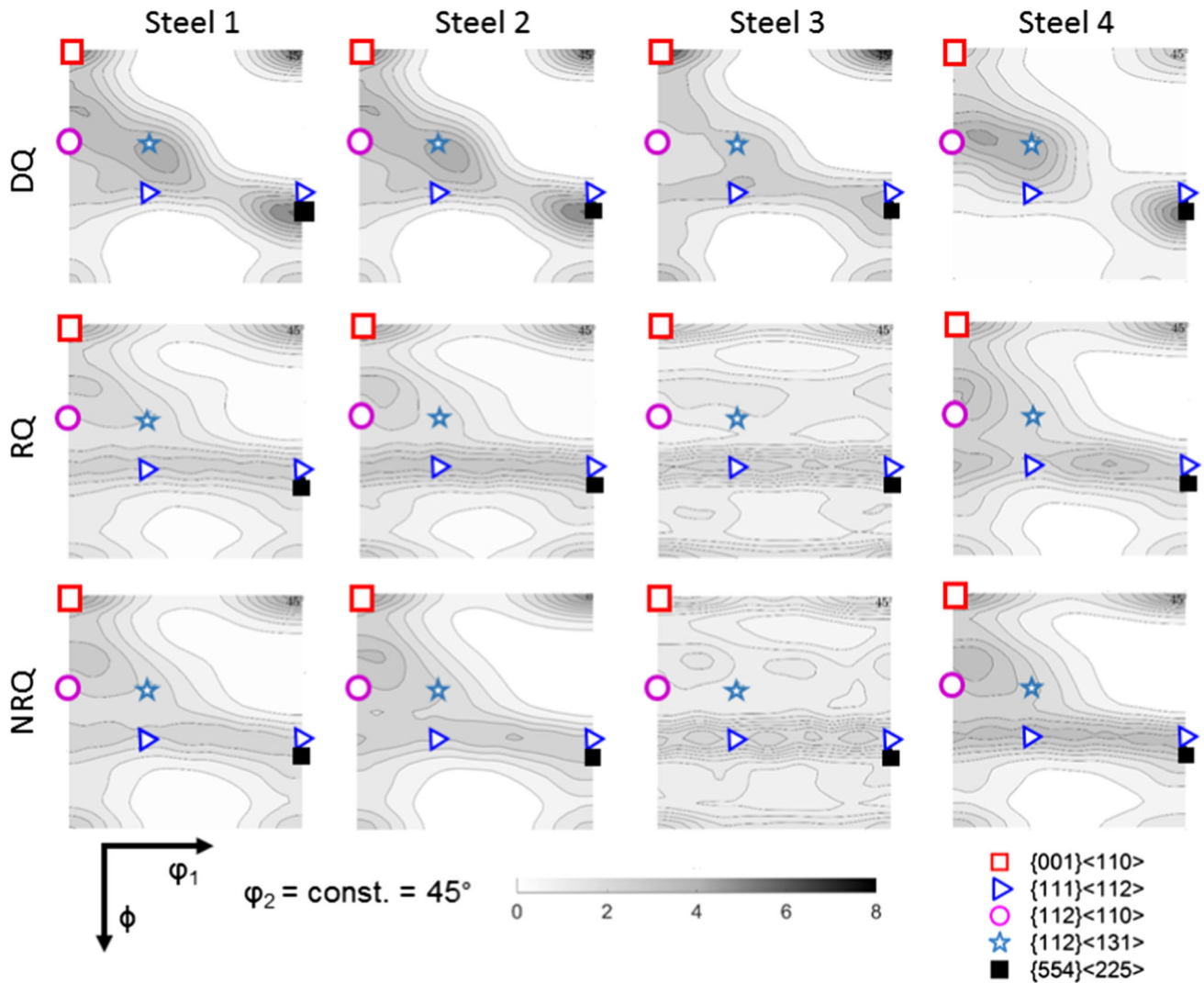


Figure 6 ODF sections at $\phi_2 = 45^\circ$ demonstrating the textures at one-fourth of the sheet depth for steels 1–4 in DQ, RQ and NRQ condition. Steel 3 possesses a weak preferential orientation after

re-austenitization, which almost disappear after normalization + quenching (NRQ). Steel 4 even shows after two time austenitization augmented texture fibers. sub-block and block boundaries [8, 48, 49]. It was observed that the fraction of the misorientation at 6.5° of steels 2 and 4 is increased during re-austenitization compared to the direct-quenched variants. Due to the fact that steel 3 does not exhibit this phenomenon but rather shows an unchanged distribution at 6.5° between DQ and RQ, this difference can be attributed to the pancaking of the PAGs due to the MAE of steels 2 and 4. After RQ, the equiaxed PAGs of steels 2 and 4 contribute to an increase in the low-angle grain boundaries. The PAGs of steel 3 are already equiaxed after DQ, so that a change of the frequency does not occur. Furthermore, also the high-angle grain boundaries at 59.5° show an increase after re-

re-austenitization, which almost disappear after normalization + quenching (NRQ). Steel 4 even shows after two time austenitization augmented texture fibers.

austenitization. Nevertheless, these differences are too little to contribute to an explication for a remaining anisotropy.

Consequently, there is still a missing link of the remaining anisotropy which in case of steels 3 and 4 cannot be eliminated completely, and therefore, measurements of the texture were taken. EBSD reaches its limit if the detected microstructure is very small as for the present case [50]. For a proper texture analysis, at least 10.000 grains are suggested to be measured [51]. The step size needs to be reduced immensely when detecting microstructures with high grain boundary densities, as it is the case for martensitic steels. This would result in an extremely

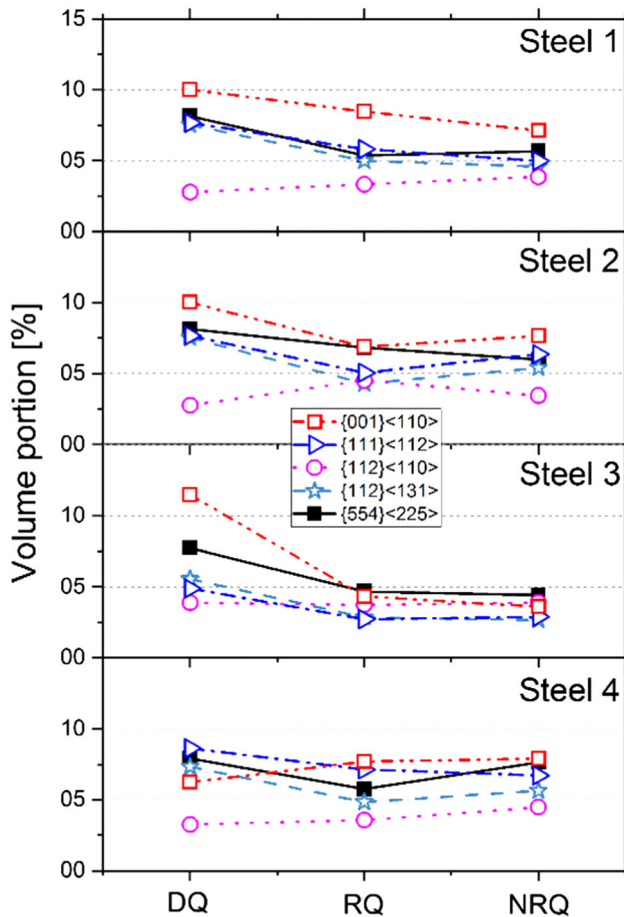


Figure 7 Effect of the different hardening procedures on the texture components of the investigated steels calculated through MTEX based on the obtained pole figures. Decreasing textures can be observed during re-austenitization of steels 1–3, and steel 4 exhibits texture remnants; however, the proportions change after re-austenitization.

high effort for textures analysis with EBSD. The XRD measurements, however, provided the orientation distributions over the whole sample for the relevant sheet position of 1.5 mm below the surface. The orientations of interest and their distributions are highlighted in Figs. 6 and 7. All steels investigated contain a decisive fraction of the $\{001\} \langle 110 \rangle$ component, especially steels 1–3 after DQ from the rolling heat. This orientation arises from the recrystallized austenite cube texture [52, 53] and thus is sparsely present in steel 4 which is alloyed with strong recrystallization retarding elements (Nb) preventing a recrystallization prior to transformation. The $\{001\} \langle 110 \rangle$ texture is known to be unfavorable for impact toughness and provokes delamination and crack propagation [52, 54]. However, a clear link to the $A_V/$

T diagram in Fig. 3 cannot be made. Despite a decrease in the intensity of $\{001\} \langle 110 \rangle$ (Fig. 7), the Charpy impact toughness of steels 1 and 2 decreases too and already falls after NRQ below 50 J at a temperature of 0 °C. These values are even lower than the values measured for steel 3, although a higher toughness is expected for steel 4 according the diametrical trend of strength and ductility. The prevailing components in steel 3 after DQ are $\{111\} \langle 112 \rangle$, $\{112\} \langle 110 \rangle$ and $\{112\} \langle 131 \rangle$ which emerge from a deformed austenite [29]. The latter ranks as a very stable orientation for higher toughness toward the rolling direction [31, 33, 52–54]. Furthermore, all steels contain significant fractions of $\{554\} \langle 225 \rangle$ arising as well from a strongly deformed γ grain [20, 52]. This component is inherited to RQ and even present after NRQ. The relatively high proportions of the $\{001\}$ sheet plane component in the DQ condition of steels 1–3 might explain differences between L and T . This is confirmed by the fact that a reduction in the $\{001\} \langle 110 \rangle$ partitions reduces the impact toughness anisotropy after RQ. However, the question remains, why an almost levelled-out texture distribution as it exists in steel 3 after re-austenitization (Figs. 6 and 7) still delivers small but present differences between L and T . And in contrast to that, steel 4 which exhibits a significant amount of defined texture components even after HRQ exhibits excellent Charpy impact values in each condition (DQ and RQ) with a relatively small anisotropy. Consequently, a clear link between a remaining anisotropy and prevailing textures thus cannot be made with certainty. Furthermore, a strict distinction whether a mechanical anisotropy can be attributed to an elongated γ grain, texture fractions or nonmetallic inclusions [23] is not possible. In a previous publication [10], it was found that variances in the FRT can even affect the properties of $Q + T$ steels, contrary to the assumption that the FRT has no effect on the properties of steels which are later re-austenitized and quenched. The present investigations confirm these findings, in specific, that the relation of FRT and T_{NR} not only plays a major role during TMP but rather influences the mechanical properties through the inheritance of microstructural characteristics. Although the usage of MAE provokes through a highly deformed γ grain a mechanical anisotropy, this does not mean simultaneously that the microstructural cancellations of these peculiarities are the key to a mechanical isotropy. Rather it can be observed that the higher the pancaking is, the

more intense is the inheritance of the properties of the prior process steps.

Summary

In order to study the dependency of the mechanical anisotropy on the microstructure, four low-C UHS steels were subjected to varying austenitization conditions prior to hardening. The results described above have shown that through thermomechanical rolling microstructural peculiarities remain in the material, which are responsible for differences between the longitudinal and transverse directions. This mechanical anisotropy cannot be eliminated entirely through re-austenitization. The main findings are summarized in the following:

- Differences in the impact toughness between the longitudinal and transverse directions can be lowered through re-austenitization or normalization prior to quenching. However, this improvement reduces the yield strength and impact toughness significantly. The microstructural benefits which are accompanied by thermomechanical processing such as a grain refinement through a highly deformed γ grain are extinguished through re-austenitization.
- The mechanical anisotropy can partially be contributed to texture components, which are promoted by hot rolling. These preferential orientations arise either from a recrystallized austenite such as $\{001\} \langle 110 \rangle$ or through a deformed γ grain such as $\{111\} \langle 112 \rangle$, $\{112\} \langle 110 \rangle$ or $\{112\} \langle 131 \rangle$. The $\{554\} \langle 225 \rangle$ component, which was also observed arise from a highly deformed austenite and is inherited to quenching after re-austenitization and even present after normalization.
- A fine γ grain as a result of Nb micro-alloying consolidates the aforementioned texture components and prevents their decimation after re-austenitization.
- The microstructural inheritance through thermomechanical rolling cannot be erased through re-austenitization or normalization. The effect of this inheritance is dependent on the intensity of the TM program, in specific, the usage of MAE and the reduction in the non-recrystallization regime.

Acknowledgements

Open access funding provided by Montanuniversität Leoben. Funding of the Austrian BMVIT in the framework of the program “Production of the future,” the Austrian Federal Ministry for Digital and Economic Affairs, the National Foundation for Research, Technology and Development as well as the “BMVIT Professorship for Industry” is gratefully acknowledged. Further, we sincerely thank the voestalpine Stahl AG, who provided the steel samples for the present investigations.

Funding

Funding was provided by Österreichische Forschungsförderungsgesellschaft (Grant No. 846933).

Compliance with ethical standards

Conflict of interest The authors declare no conflict of interest.

Open Access This article is distributed under the terms of the Creative Commons Attribution 4.0 International License (<http://creativecommons.org/licenses/by/4.0/>), which permits unrestricted use, distribution, and reproduction in any medium, provided you give appropriate credit to the original author(s) and the source, provide a link to the Creative Commons license, and indicate if changes were made.

References

- [1] Tamura I (ed) (1988) Thermomechanical processing of high-strength low-alloy steels. Butterworths, London
- [2] Klein M, Rauch R, Spindler H, Stiaszny P (2012) Ultra high strength steels produced by thermomechanical hot rolling—advanced properties and applications. BHM 157:108–112
- [3] Klein M, Spindler H, Luger A, Rauch R, Stiaszny P, Eigelsberger M (2005) Thermomechanically hot rolled high and ultra high strength steel grades—processing, properties and application. Mater Sci Forum 500–501:543–550
- [4] Hodgson PD, Beladi H, Barnett MR (2005) Grain refinement in steels through thermomechanical processing. Mater Sci Forum 500–501:39–48

- [5] Banerjee MK, Banerjee PS, Datta S (2001) Effect of thermomechanical processing on the microstructure and properties of a low carbon copper bearing steel. *ISIJ Int* 41:257–261
- [6] Cuddy LJ (1981) The effect of microalloy concentration on the recrystallization of austenite during hot deformation. In: DeArdo AJ, Ratz GA, Wray PJ (eds) *Thermomechanical processing of microalloyed austenite*. Metallurgical Society of AIME, Warrendale, pp 129–140
- [7] Ouchi C (2001) Development of steel plates by intensive use of TMCP and direct quenching processes. *ISIJ Int* 41:542–553
- [8] Kajjalainen A, Pallaspuuro S, Porter DA (2014) Tempering of direct quenched low-alloy ultra-high-strength steel, part I—microstructure. *Adv Mater Res* 922:316–321
- [9] Kajjalainen AJ, Suikkanen PP, Linnell TJ, Karjalainen LP, Kömi JI, Porter DA (2013) Effect of austenite grain structure on the strength and toughness of direct-quenched martensite. *J Alloys Compd* 577:642–648
- [10] Esterl R, Sonnleitner M, Gschöpf B, Schnitzer R (2019) Influence of V and Nb micro-alloying on direct quenched and tempered ultra-high strength steels. *Steel Res Int*. <https://doi.org/10.1002/srin.201800640>
- [11] Hensger KE, Bernštejn ML (1984) *Thermomechanische Veredlung von Stahl*. VEB Deutscher Verlag für Grundstoffindustrie, Berlin
- [12] Bracke L, Xu W, Waterschoot T (2015) Effect of finish rolling temperature on direct quenched low alloy martensite properties. *Mater Today Proc* 2:659–662
- [13] Kajjalainen A, Vähäkuopus N, Somani M, Mehtonen S, Porter D, Kömi J (2017) The effects of finish rolling temperature and niobium microalloying on the microstructure and properties of a direct quenched high-strength steel. *Arch Metall Mater* 62:619–626
- [14] Kajjalainen AJ, Suikkanen PP, Karjalainen LP, Porter DA (2016) Influence of subsurface microstructure on the bendability of ultrahigh-strength strip steel. *Mater Sci Eng A* 654:151–160
- [15] Deardo AJ (2003) Niobium in modern steels. *Int Mater Rev* 48:371–402
- [16] Dutta B, Sellars CM (1986) Strengthening of austenite by niobium during hot rolling of Microalloyed steel. *Mater Sci Technol* 2:146–153
- [17] Swarr T, Krauss G (1976) The effect of structure on the deformation of as-quenched and tempered martensite in an Fe-0.2 pct C alloy. *Metall Trans A* 7:41–48
- [18] Krauss G, Marder AR (1971) The morphology of martensite in iron alloys. *Metall Trans* 2:2343–2357
- [19] Davies RG, Magee CL (1971) Influence of austenite and martensite strength on martensite morphology. *Metall Trans* 2:1939–1947
- [20] Kajjalainen AJ, Suikkanen P, Karjalainen LP, Jonas JJ (2014) Effect of austenite pancaking on the microstructure, texture, and bendability of an ultrahigh-strength strip steel. *Metall Mater Trans A* 45:1273–1283
- [21] Pereda B, Lopez B, Rodriguez-Ibabe JM (2007) Increasing the non-recrystallization temperature of Nb microalloyed steels by Mo addition. *Int Conf Microalloyed Steels Process Microstruct Prop Perform Proc* 2007:151–159
- [22] Vervynckt S, Verbeken K, Lopez B, Jonas JJ (2012) Modern HSLA steels and role of non-recrystallisation temperature. *Int Mater Rev* 57:187–207
- [23] Joo MS, Suh DW, Bhadeshia HKDH (2013) Mechanical anisotropy in steels for pipelines. *ISIJ Int* 53:1305–1314
- [24] Kajjalainen A, Karjalainen P, Porter D, Suikkanen P, Kömi J, Kesti V, Saarinen T (2012) Effect of inclusions on the properties of ultra-high-strength low-alloy steel with a martensitic-bainitic microstructure. In: *Proceedings of the 8th international conference on clean steel*. Budapest, Hungary, p 10
- [25] Courbon J, Lormand G, Dudragne G, Daguier P, Vincent A (2003) Influence of inclusion pairs, clusters and stringers on the lower bound of the endurance limit of bearing steels. *Tribol Int* 36:921–928
- [26] Imai T, Nishida Y, Kogiso S (1982) Anisotropy of the charpy impact value of carbon steels and corrective heat treatment. *J Mech Work Technol* 7:147–161
- [27] Sokolov BK, Sadovskii VD (1959) Mechanism of austenite formation in heating steel. *Met Sci Heat Treat* 1:7–14
- [28] Sharma M, Bleck W (2018) Study of structural inheritance of austenite in Nb-Microalloyed 18CrNiMo7-6 steel. *Steel Res Int*. <https://doi.org/10.1002/srin.1800107>
- [29] Raabe D (2003) Overview on basic types of hot rolling textures of steels. *Steel Res Int* 74:327–337
- [30] Misra RDK, Nathani H, Siciliano F, Carneiro T (2004) Effect of texture and microstructure on resistance to cracking of high-strength hot-rolled Nb–Ti microalloyed steels. *Metall Mater Trans A* 35:3024–3029
- [31] Bleck W, Grossterlinden R, Lotter U, Reip C-P (1991) Textures in steel sheets. *Steel Res* 62:580–586
- [32] Haskel HL, Pauletti E, de Martins JP, de Carvalho ALM (2014) Microstructure and microtexture assessment of delamination phenomena in charpy impact tested specimens. *Mater Res* 17:1238–1250
- [33] Joo MS, Suh D-W, Bae JH, Sanchez Mouriño N, Petrov R, Kestens LAI, Bhadeshia HKDH (2012) Experiments to separate the effect of texture on anisotropy of pipeline steel. *Mater Sci Eng A* 556:601–606

- [34] Gladman T (1997) The physical metallurgy of microalloyed steels. Institute of Materials, London
- [35] Bhadeshia H, Honeycombe R (2017) Chapter 4—solutes that substitute for iron. In: Bhadeshia H, Honeycombe R (eds) Steels microstructure and properties, 4th edn. Butterworth-Heinemann, Oxford, pp 101–134
- [36] Totten GE (2006) Steel heat treatment: metallurgy and technologies, 2nd edn. CRC Press, Portland
- [37] Brooks CR (1996) Principles of the heat treatment of plain carbon and low alloy steels, 1st edn. ASM International, Materials Park
- [38] Babcock WR, Wilcox (1995) A review of steels: metallurgy and applications by D.T. Llewellyn. Mater Manuf Process 10:330–331
- [39] Andrade HL, Akben MG, Jonas JJ (1983) Effect of molybdenum, niobium, and vanadium on static recovery and recrystallization and on solute strengthening in microalloyed steels. Metall Trans A 14:1967–1977
- [40] Lagneborg R, Siwecki T, Zajac S, Hutchinson B (1999) The role of vanadium in microalloyed steels. Scand J Met 28:186–241
- [41] Bhadeshia H, Honeycombe R (2017) Chapter 9—tempering of martensite. In: Bhadeshia H, Honeycombe R (eds) Steels microstructure and properties, 4th edn. Butterworth-Heinemann, Oxford, pp 237–270
- [42] Gottstein G (2007) Physikalische Grundlagen der Materialkunde, 3rd edn. Springer, Berlin
- [43] Esterl R, Sonnleitner M, Schnitzer R (2019) Microstructural analysis of the recrystallization behavior of low alloyed steels. Steel Res Int 90:382–391
- [44] Österle W (1981) Textur- und Gefügeentwicklung beim Walzen von polykristallinem alpha-Eisen. Textur- und Gefügeentwicklung beim Walzen von polykristallinem alpha-Eisen. PhD Thesis
- [45] Bachmann F, Hielscher R, Schaeben H (2010) Texture analysis with MTEX, a free and open source software Toolbox, In: Klein H, Schwarzer RA (eds) Texture anisotropy polycrystals III. Trans Tech Publications, pp 63–68
- [46] Medina SF (1998) Determination of no-recrystallisation temperature in Nb–V–Ti microalloyed steel and discussion of its definition. Mater Sci Technol 14:217–221
- [47] Thelning K-E (1967) Steel and its heat treatment. Butterworth-Heinemann, Oxford
- [48] Morito S, Tanaka H, Konishi R, Furuhashi T, Maki T (2003) The morphology and crystallography of lath martensite in Fe–C alloys. Acta Mater 51:1789–1799
- [49] Morito S, Huang X, Furuhashi T, Maki T, Hansen N (2006) The morphology and crystallography of lath martensite in alloy steels. Acta Mater 54:5323–5331
- [50] Esterl R, Sonnleitner M, Stadler M, Wölger G, Schnitzer R (2018) Microstructural characterization of ultra-high strength martensitic steels. Pract Metallogr 55:203–222
- [51] Wright SI, Nowell MM, Bingert JF (2007) A comparison of textures measured using X-ray and electron backscatter diffraction. Metall Mater Trans A 38:1845–1855
- [52] Ray RK, Jonas JJ, Butrón-Guillén MP, Savoie J (1994) Transformation textures in steels. ISIJ Int 34:927–942
- [53] Suwas S, Ray RK (2014) Crystallographic texture of materials. Springer, London. <https://doi.org/10.1007/978-1-4471-6314-5>
- [54] Yang X-L, Xu Y-B, Tan X-D, Wu D (2015) Relationships among crystallographic texture, fracture behavior and Charpy impact toughness in API X100 pipeline steel. Mater Sci Eng A 641:96–106

Publisher's Note Springer Nature remains neutral with regard to jurisdictional claims in published maps and institutional affiliations.